Research Article

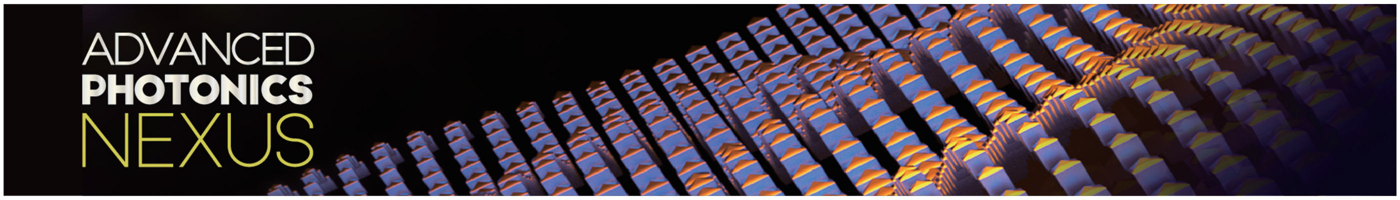

ADVANCED PHOTONICS NEXUS

Light-induced vacuum micromotors based on an antimony telluride microplate

Weiwei Tang,[a,b,c,*] **Qiannan Jia,**[b,c] **Yong Wang,**[b,c] **Ding Zhao,**[b,c] **Wei Lyu,**[b,c] **Wei Yan,**[b,c,*] **and Min Qiu**[b,c,*]
[a]University of Chinese Academy of Sciences, Hangzhou Institute for Advanced Study, College of Physics and Optoelectronic Engineering, Hangzhou, China
[b]Westlake University, School of Engineering, Key Laboratory of 3D Micro/Nano Fabrication and Characterization of Zhejiang Province, Hangzhou, China
[c]Institute of Advanced Technology, Westlake Institute for Advanced Study, Hangzhou, China

Abstract. Manipulating motion of microobjects with light is indispensable in various technologies. On solid interfaces, its realizations, however, are hampered by surface friction. To resolve this difficulty, light-induced elastic waves have been recently proposed to drive microobjects against friction. Despite its expected applicability for arbitrary optical-absorptive objects, the new principle has only been tested with microsized gold plates. Herein, we validate this principle using a new material and report directional and continuous movements of a two-dimensional topological insulator (Sb_2Te_3) plate on an untreated microfiber surface driven by nanosecond laser pulses. The motion performance of the Sb_2Te_3 plate is characterized by a scanning electron microscope. We observe that the motion velocity can be controlled by tuning the average power of laser pulses. Further, by intentionally increasing the pulse repetition rate and exploiting the low thermal conductivity of Sb_2Te_3, we examine the thermal effects on actuation and reveal the motion instability induced by formations of microbumps on Sb_2Te_3 surfaces due to the Marangoni effects. Moreover, as the formed microbumps are heated to viscoelasticity states, liquid-like motion featuring asymmetry in contact angles is observed and characterized, which expands the scope of light-induced actuation of microobjects.

Keywords: optical actuation; nonliquid environment; topological insulator.

Received Oct. 10, 2022; accepted for publication Oct. 18, 2022; published online Nov. 16, 2022.

[DOI: 10.1117/1.APN.1.2.026005]

1 Introduction

Motion is everywhere in living systems and is necessary for mechanical functions in artificial systems, such as robots and machines. Functional mechanical structures that change volume and shape and move in response to external stimuli, including chemical, electrical, or optical forces, are essential in various applications.[1–5] They have received immense research interest, particularly at micro-/nanoscales. Among the existing actuation proposals, many rely on light as the energy source. Optical force is thus widely used to manipulate microobjects that are either immersed in a liquid or levitated in a vacuum.[6–11]

It is, however, challenging to use the optical force to manipulate microobjects on solid interfaces due to surface friction that is typically several orders of magnitude larger ($\sim\mu N$) than the optical force ($\sim pN$).[4,6,12–15] To resolve this difficulty, it has been recently proposed to use elastic waves,[16–22] which are induced by temperature rising through optical absorption in microobjects.[16–20] These light-induced elastic waves carry sufficient mechanical displacements enabling microobjects to crawl on solid interfaces. The idea has been successfully exemplified with gold microplates in microfiber-based systems.[16–20] Specifically, the researchers have successfully observed the stable motion of gold plates around microfibers along either or both of azimuthal and axial directions of the microfibers. The motion speed increases with the average power of input laser pulses. These pioneering results encouragingly open a new perspective for light-driven micromotors on solid interfaces. Many unique applications can be immediately envisioned. For instance, by integrating this technique into an on-chip waveguide network, one can realize mobile photonic modulation/

---

*Address all correspondence to Weiwei Tang, tangweiwei@ucas.ac.cn; Wei Yan, wyanzju@gmail.com; Min Qiu, qiumin@westlake.edu.cn

switching by delivering microobjects to targeted positions[18] to control light flow.

Notwithstanding recent advancements in this new direction, there still remain several questions to be explored.

1. As argued in Refs. 17 and 19, the actuation principle is theoretically applicable for any microobjects as long as they can generate elastic waves by absorbing light. However, it has only been tested with gold microplates, and has not yet been extended to other absorptive, elastic materials.
2. Since elastic waves are excited by optical absorption, potential issues associated with thermal effects (such as thermal damage and melting) should be addressed.

Here we approach these two questions by studying the motion of two-dimensional topological-insulator Sb_2Te_3 plates on microfibers to which laser pulses are delivered. Sb_2Te_3 is a unique quantum material hosting topologically protected boundary surface states that lead to several fascinating electronic and optical properties, such as spin-momentum locking of electrons and ultrabroadband plasmon excitations.[23–26] Referring to our objectives, we utilize its two other properties. First, Sb_2Te_3 is a narrow-gap semiconductor with only a 0.21 eV bandgap,[27] thus being efficient at absorbing light for the generation of elastic waves. Second, Sb_2Te_3 has a rather low thermal conductivity ($\sim 1\ \mathrm{W\,m^{-1}\,K^{-1}}$, close to glass and two orders of magnitude smaller than that of gold), which mitigates heat diffusion and intensifies thermal effects.[28]

In this paper, we implement a microfiber-based actuation system in a vacuum chamber. A scanning electron microscope (SEM) is employed to precisely characterize pulsed light-induced actuation of microsized Sb_2Te_3 plates on microfibers. The successful observations of continuous spiral motions of Sb_2Te_3 plates supplement the previous ones with gold plates, and thus contributes new evidence to support the actuation principle based on light-induced elastic waves. Further, we intentionally increase laser power to examine thermal effects on actuation. Specifically, we show formations of microbumps due to the Marangoni effects on a Sb_2Te_3 surface and observe a new type of liquid-like motion that shows features completely different from the elastic-waves-based spiral motion.

2 Light-Induced Actuation

As illustrated in Fig. 1(a), a Sb_2Te_3 plate is placed on a suspended silica microfiber. A supercontinuum light (wavelength range from 450 to 2400 nm) is launched into the microfiber to drive the locomotion of the plate. The experimental setup is similar as that used for actuating gold plates in our previous work.[17,19] The Sb_2Te_3 plate was obtained by mechanical exfoliation using dicing tape and then dispersed on a SiO_2 (300 nm) thin film on a Si substrate. The confocal laser scanning microscopy images [see the inset in Fig. 1(b) and, similarly, Fig. S1 in the Supplementary Material] show that the plate considerably warps around its edges. The plate was transferred onto the microfiber using a tapered fiber. The thickness of the plate varies between 0.2 and 1.5 μm. We measured the Sb_2Te_3 plate by micro-Raman spectroscopy (Alpha300R) with 532-nm-laser light. The Raman spectrum [Fig. 1(b)] shows three characteristic peaks at 68.26, 112.45, and 165.36 $\mathrm{cm^{-1}}$, respectively, which correspond to A^1_{1g}, E^2_g, and A^2_{1g} phonon vibrational modes of Sb_2Te_3.[30]

The presence of nontrivial topological surface states renders the Sb_2Te_3 plate a multilayer character;[31] that is, a dielectric bulk slab is sandwiched between two metallic surface layers [see the zoomed inset in Fig. 1(a)]. The permittivity of the metallic surface layers and the insulating bulk of the Sb_2Te_3 plate is adopted from Ref. 29 and is plotted in Fig. S2 in the Supplementary Material. However, due to their negligible thickness (2.6 nm), the metallic layers only slightly impact the optical absorption of the Sb_2Te_3 plate (see Fig. S3 in the Supplementary Material). Consider that a fundamental $\mathrm{HE}_{11}^{\perp}$ mode (linearly polarized perpendicular to the plate surface) propagates in a microfiber with a diameter of 4 μm and interacts with a rectangular Sb_2Te_3 plate (width: 3 μm, length: 12 μm, and thickness: 300 nm). The calculated absorption spectrum is plotted in Fig. 1(c), showing an average absorptance of about 0.15. Figure 1(d) compares $\mathrm{HE}_{11}^{\perp}$ modal profiles with and without the Sb_2Te_3 plate. Interestingly, in the presence of the Sb_2Te_3 plate, the displacement electric field in the plate strongly localizes around the touching point between the plate and the microfiber, where the most absorption occurs. This field profile manifests strong near-field interactions between the electric polarization in the microfiber and its induced mirror image inside the plate. Furthermore, since the near-field interactions are polarization sensitive, those modes, which host weak interactions such as the fundamental $\mathrm{HE}_{11}^{\parallel}$ mode (linearly polarized parallel with the plate surface), are negligibly absorbed (see Fig. S3 in the Supplementary Material).

The absorbed optical power generates heat. The heat diffusion in the Sb_2Te_3 plate is rather slow. More precisely, the thermal diffusivity of Sb_2Te_3 is only about $\alpha_{\mathrm{Sb_2Te_3}} \simeq 10^{-6}\ \mathrm{m^2/s}$, while this value for gold is $\alpha_{\mathrm{Au}} \simeq 10^{-4}\ \mathrm{m^2/s}$, two orders of magnitude larger. Quantitatively, to transport heat diffusively across a Sb_2Te_3 plate with side length $L \sim 10\ \mu\mathrm{m}$ (similar to that in our experiments), it roughly takes time $L^2/\alpha_{\mathrm{Sb_2Te_3}} \sim 100\ \mu\mathrm{s}$. In contrast, for the same-sized gold plate, this time is significantly reduced to $L^2/\alpha_{\mathrm{Au}} \sim 1\ \mu\mathrm{s}$. Hence, inside the Sb_2Te_3 plate, the absorbed heat could be efficiently stored in vicinity to the contact line between the plate and the microfiber, where the optical absorption is maximum; whereas inside the Au plate, the initially localized heat rapidly spreads throughout the plate, as validated with the numerical simulations in Fig. 1(e). The slow heat diffusion in the Sb_2Te_3 plate is naturally envisioned to boost noticeable thermal effects, as shall be experimentally examined later.

The temperature rising in the Sb_2Te_3 plate excites elastic waves, which drive the locomotion of the plate on the microfiber. The underlying mechanisms, featuring interplay between elastic waves and their induced friction force, have been comprehensively studied in our previous work, and we refer the interested reader to Refs. 17, 19, and 20.

We characterized the motion of the Sb_2Te_3 plate using a SEM in a vacuum chamber [see Fig. 2(a)]. The SEM here brings two advantages. First, it provides a much better spatial resolution compared with the use of an optical microscope. Second, due to the high-vacuum environment ($<10^{-3}$ Pa), those less important effects, e.g., due to surrounding gas molecules (including photophoretic forces and air resistances), on actuation are safely screened out, thus simplifying the physics interpretation. In addition, we also conducted the experiments at ambient conditions and arrived at similar observations as in vacuum.

Figure 2(b) plots sequencing SEM images of a Sb_2Te_3 plate that crawls along a microfiber following a spiral trajectory (also see Video 1). We characterized the spiral motion by decomposing it into the rotation and the translation along the azimuthal

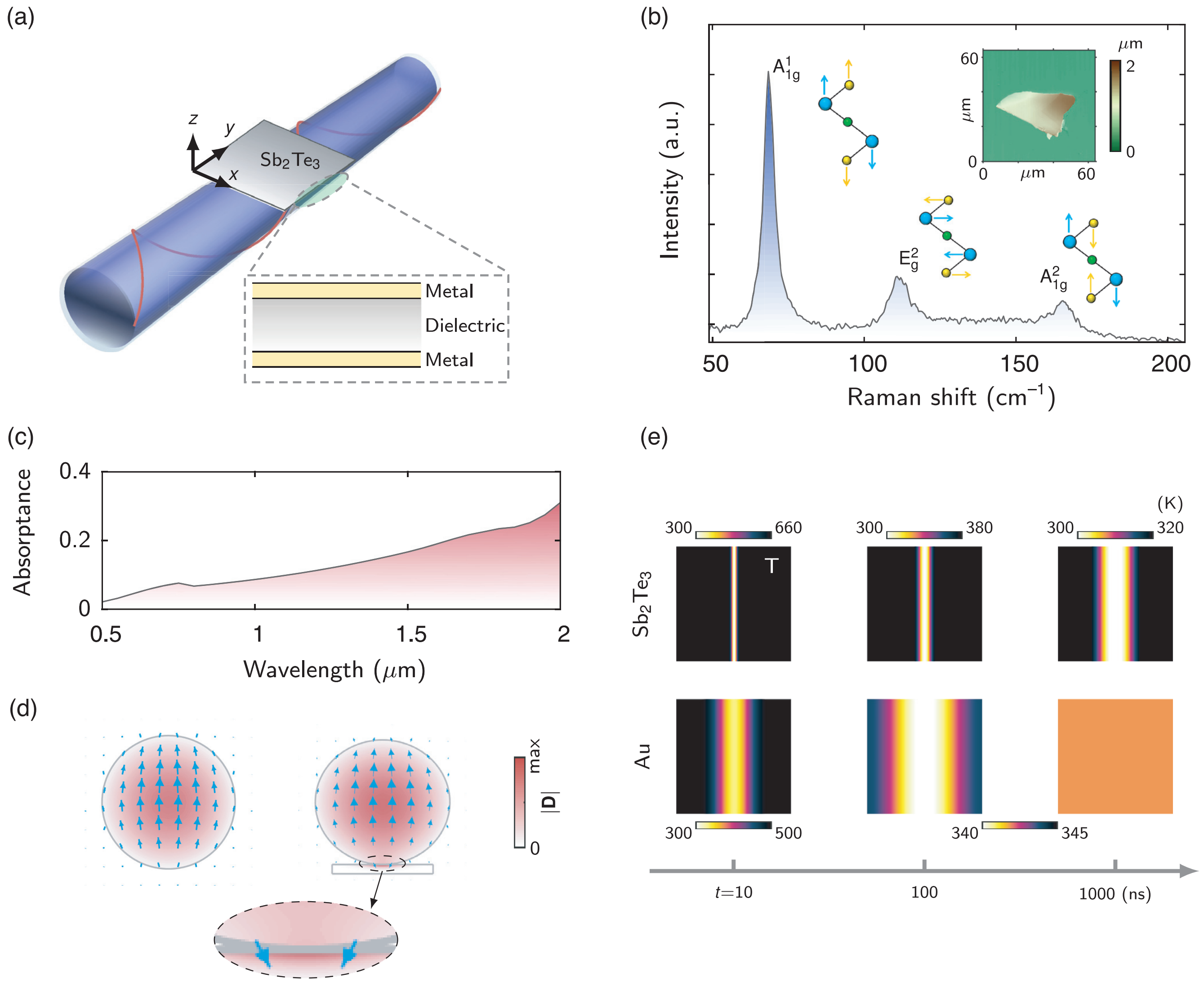

Fig. 1 Optical and thermal properties of hybrid Sb_2Te_3 plate–silica microfiber systems. (a) Sketch of a Sb_2Te_3 plate on top of a suspended microfiber. Zoomed inset: a Sb_2Te_3 plate is modeled as a dielectric bulk slab sandwiched between two metallic thin layers. (b) Micro-Raman spectrum of a Sb_2Te_3 plate measured by a 532-nm pumping laser. Inset: confocal laser scanning microscopy image of a mechanical-exfoliated Sb_2Te_3 plate on a SiO_2/Si substrate. (c) Simulated absorption spectrum of a hybrid Sb_2Te_3 plate–microfiber system under incidence of fundamental $HE^{\perp}_{11}$ mode of the microfiber. (d) Simulated modal profiles of the $HE^{\perp}_{11}$ mode without (left panel) and with (right panel) the Sb_2Te_3 plate. The arrows specify the directions of modal electric fields. (e) Simulated characteristic temperature distributions in the central $x-y$ plane of Sb_2Te_3 and gold plates at $t = 10$, 100, 1000 ns when heated by pulsed light. In (c)–(e), the microfiber has a radius of 2 μm and a refractive index of 1.45. The Sb_2Te_3 plate has a width of 3 μm, a length of 12 μm, and a thickness of 300 nm, and its surface and bulk refractive indices are adopted from Ref. 29. The Au plate has the same geometrical parameters as the Sb_2Te_3 plate. The details of the thermal simulations in (e) are given in Note S1 in the Supplementary Material.

and axial directions of the microfiber separately. The azimuthal rotation frequency is obtained by the Fourier transformation of the effective area of the plate, which changes periodically over time. On average, the rotation frequency is estimated to be about 0.177 Hz [see Fig. 2(c)], indicating a traveling distance of 12.8 nm along the azimuthal direction per pulse on average. Figure 2(d) analyzes the axial displacement. The trajectory curve is fitted well with a straight line, and the velocity is determined to be 1.42 μm/s, implying a translation distance of 6.9 nm along the axial direction per pulse on average.

3 Remarks on Actuation Efficiency

We experimentally observe that a Sb_2Te_3 plate can be driven much more efficiently than a similarly sized gold plate[17,19,20] under irradiation of the same light pulses. For instance, as is shown in Fig. 2, when a single nanosecond light pulse with

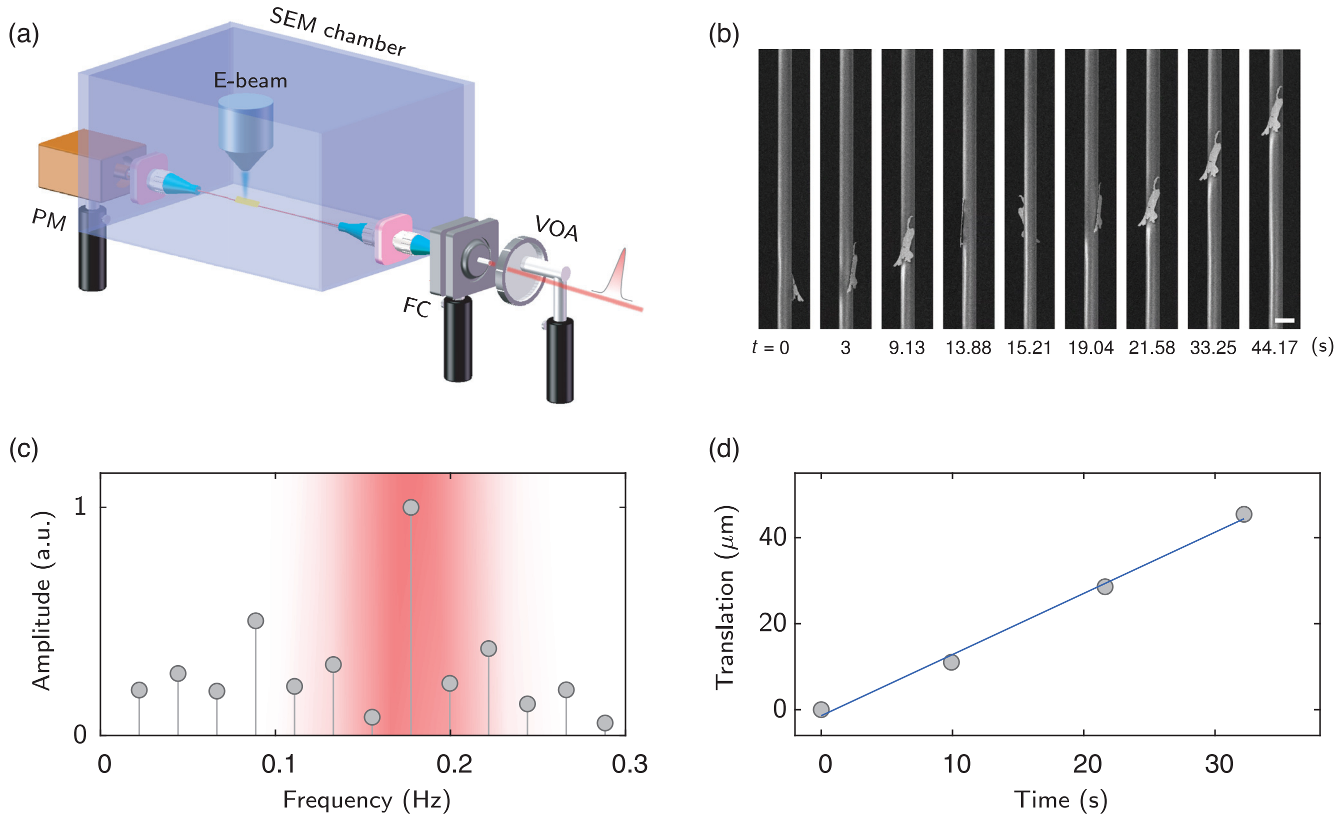

Fig. 2 Experimental observations of a Sb_2Te_3 plate moving spirally around a microfiber. (a) Sketch of experimental setup implemented in a vacuum chamber. VOA, variable optical attenuator; FC, fiber coupler; MF, microfiber; and PM, power meter. (b) Temporal sequencing SEM images of a Sb_2Te_3 plate moving around a microfiber. The microfiber has a diameter of 5 μm. The supercontinuum laser pulses have 2.6-ns duration, 230-Hz repetition rate, 0.1-mW average power, and wavelength range from 450 to 2400 nm. Scale bar: 5 μm (Video 1, MP4, 4.34 MB [URL: https://doi.org/10.1117/1.APN.1.2.026005.s1). (c) Fourier transformation of the detected areas of the Sb_2Te_3 plate during the motion. The spectral peak specifies the azimuthal rotation frequency of the plate. The Y axis is linear and the shaded region here is to better show its rotation frequency. (d) Translation displacement of the Sb_2Te_3 plate along the axial direction of the microfiber as a function of time.

a 0.43 nJ pulse energy is delivered, the Sb_2Te_3 plate travels on average about 6.9 and 12.8 nm in the axial and azimuthal directions of the microfiber, respectively. In contrast, to enable the gold plate to travel a similar distance, a much larger pulse energy (at least several times or even dozens of times larger, which are sample dependent) is needed.[19] Furthermore, from numerous repetitive tests, we consistently notice that the Sb_2Te_3 plates generally require a lower threshold pulse energy to enable their motion than the gold plates. These intuitive observations suggest that, compared with the gold plates, the Sb_2Te_3 plates have a higher actuation efficiency.

To reveal the material difference in actuation, we start with the linear elastic equation that involves both the surface friction and the thermal deformation:

$$-\frac{1-2\mu}{2(1+\mu)}\nabla\times\nabla\mathbf{u}(\mathbf{r};t)+\frac{1-\mu}{1+\mu}\nabla\nabla\cdot\mathbf{u}(\mathbf{r};t)=\frac{\rho(1-2\mu)}{E}\frac{\partial^2\mathbf{u}(\mathbf{r};t)}{\partial t^2}-\frac{1-2\mu}{E}\mathbf{f}_{\text{fric}}(\mathbf{r};t)+\alpha_{\text{th}}\nabla\delta T(\mathbf{r};t),$$

where E, μ, and ρ are the Young's modulus, Poisson's ratio, and mass density of the driven object, respectively, α_{th} is the linear expansion coefficient, $\mathbf{f}_{\text{fric}}$ is the friction force, δT is the temperature variation, and $\mathbf{u}(\mathbf{r};t)$ is the elastic displacement vector. Given by the above equation, the object displacement characterized by $\mathbf{u}(\mathbf{r};t)$ is proportional to the strength of the thermal deformation defined by $f_{\text{th}}=\alpha_{\text{th}}\delta T$, which induces the surface friction f_{fric} when the relative position between the driven object and the substrate changes in response to the thermal deformation. Consequently, the defined thermal-deformation strength f_{th} indicates the actuation efficiency (that is, a larger f_{th} principally corresponds to a higher actuation efficiency and vice versa). Specifically, when an input nanosecond light pulse is converted to heat in the driven object with an optical absorption efficiency denoted by A_{abs}, $f_{\text{th}}\sim\alpha_{\text{th}}A_{\text{abs}}/\rho c_p$, where c_p is the object's specific heat capacity. It is obvious that materials with larger A_{abs} and α_{th}, and smaller ρ and c_p are more favorable for the use of actuation than the opposite. In addition, we note that the estimation of A_{abs} cannot be directly inferred from the basic electromagnetic parameters (complex-valued permittivity and permeability), and quantitative electromagnetic simulations should be consulted [such as in Fig. 1(c)].

Referring to the Sb_2Te_3 and gold plates with similar sizes, they show close absorption efficiency A_{abs} [see Fig. 1(c) and Fig. S8c in the Supplementary Material in Ref. 19 that the average absorption between 400 nm and 2 μm wavelength is about 0.15 to 0.2 in both cases]. The other relevant parameters of such two materials are $\alpha_{\mathrm{th}}^{\mathrm{Sb_2Te_3,Au}} = 25 \times 10^{-6}$, $14.2 \times 10^{-6}\ \mathrm{K}^{-1}$, $c_p^{\mathrm{Sb_2Te_3,Au}} = 200$, 126 $\mathrm{JK^{-1}\,kg^{-1}}$, and $\rho^{\mathrm{Sb_2Te_3,Au}} = 6500$, 19,300 $\mathrm{kg\,m^{-3}}$. As a result, $f_{\mathrm{th}}^{\mathrm{Sb_2Te_3}} \simeq 3.2 f_{\mathrm{th}}^{\mathrm{Au}}$, which is mainly due to the lighter mass density and slightly larger thermal expansion coefficient of Sb_2Te_3 than those of gold, thus contributing to a higher actuation efficiency of the Sb_2Te_3 plate.

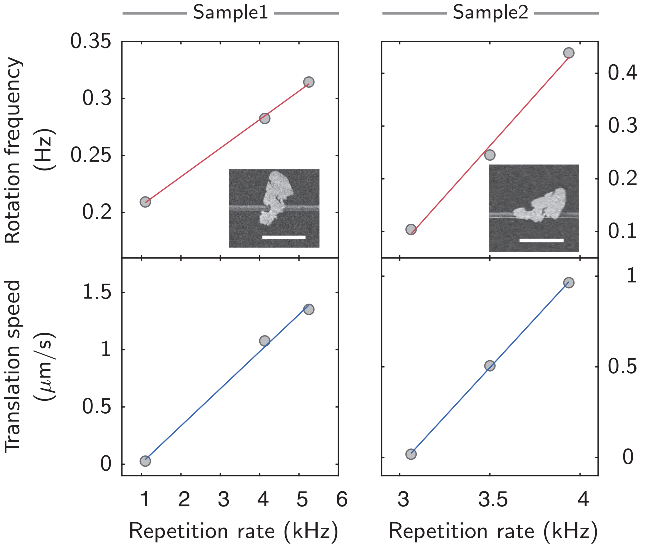

Fig. 3 Manipulating motion speed of Sb_2Te_3 plates by tuning repetition rates of laser pulses. Note that the integrated single-pulse energy remains the same as the repetition rate changes. Scale bars: 30 μm (Video 2, MP4, 19.6 MB [URL: https://doi.org/10.1117/1.APN.1.2.026005.s2]).

Moreover, we note that the thermal conductivity of Sb_2Te_3 is two orders of magnitude smaller than that of gold, which leads to their significant difference in heat diffusion. As a result, the local temperature in the contact region of the Sb_2Te_3 plate could be much higher than that of the gold plate [see Fig. 1(e)]. The high temperature (especially when approaching the melting point) is known to induce random motions of interfacial atoms and mitigate the friction, which could be another reason for the observed high actuation efficiency with the use of the Sb_2Te_3 plate; at the same time, the thermal effects in the Sb_2Te_3 plate become noticeable, as discussed below.

4 Thermal Effects

To examine the thermal effects on the motion of the Sb_2Te_3 plate, we intentionally increase the average power of the laser pulses by increasing the pulse repetition rate. Initially, when the pulse repetition rate is low (less than a few kHz), the plate generally moves stably, as shown in Fig. 4(a). The motion speed increases linearly with the repetition rate, as is shown in Fig. 3 with two samples (see Video 2). This result thus suggests that, in the stable-motion regime, the motion speed can be regularly controlled by tuning the pulse repetition rate because the motion is repeatedly driven by individual pulses in a stepwise fashion. Physically, the use of the low-repetition-rate pulses ensures that the Sb_2Te_3 plate heated by one pulse can be sufficiently cooled down before next pulse arrives, thereby denying thermal effects.

On the other hand, as the pulse repetition rate exceeds a certain threshold value, the plate starts to move unstably and to continually adjust its gesture during the motion, as shown in Fig. 4(b) and also Video 3. The threshold repetition rate, which triggers the motion instability, is observed to be sample dependent. Nevertheless, its value is consistently on the order of a few kHz. We argue that the threshold repetition rate is proportional to the reciprocal of the cooling time of the plate under single-pulse irradiation. More precisely, if the repetition rate is above the threshold value, the multi-pulse heat accumulation starts. As the accumulated temperature is close to the melting point of Sb_2Te_3, the plate shall be strongly deformed, particularly around the contact-line region where the absorbed optical power is largest. Numerically, we find that the cooling time is about

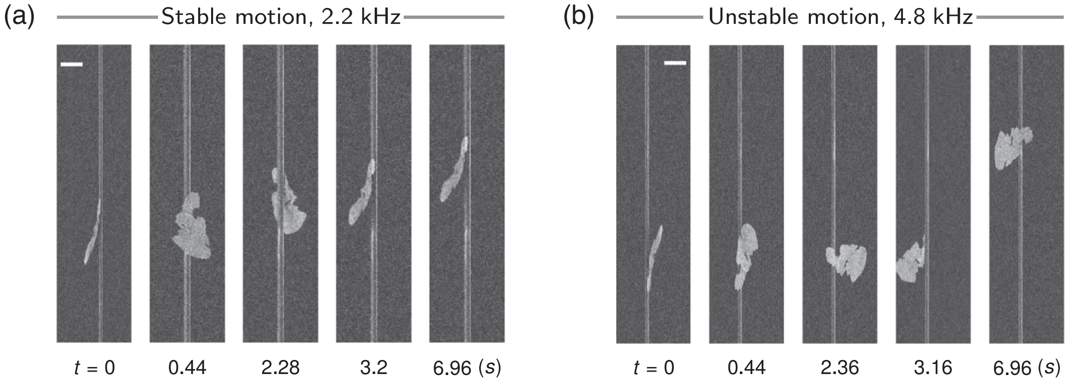

Fig. 4 Stable motion of a Sb_2Te_3 plate degenerates into unstable motion by thermal effects. Sequencing SEM images show (a) stable and (b) unstable motions with pulse repetition rates of 2.2 kHz and 4.8 kHz, respectively. Scale bars: 20 μm (Video 3, MP4, 9.73 MB [URL: https://doi.org/10.1117/1.APN.1.2.026005.s3]).

10^{-4} s, suggesting that the threshold repetition rate is about 10 kHz, close to the experimental observations.

The thermal-induced morphology dynamic changes are proposed to be responsible for the motion instability. In this regard, the formations of microbumps are one dominant phenomenon associated with the surface morphology deformations of Sb_2Te_3 under high-laser irradiance.[32] The underlying mechanism is attributed to the Marangoni effects involving both thermocapillary and chemicapillary forces. Specifically, the thermocapillary force tends to push the interfacial atoms toward the cold peripheral region with a higher surface tension. Therefore, a surface compositional gradient shall be established. In contrast, the chemicapillary force pushes the materials toward the hotter region with lower surfactant concentrations. (Note: The surfactant Te, which lowers the surface tension, can be generated by irradiation of nanosecond laser pulses, as confirmed with the Raman measurements in Fig. S4 in the Supplementary Material.) The chemicapillary and thermocapillary forces thus compete with each other. The dominance of the chemicapillary force over the thermocapillary force leads to the formations of the microbumps in the hotter region. That is, in our case, around the contact line between the plate and the microfiber, as shown in Fig. 6(b) and Video 4. The size of the microbump increases with the average power of the incident laser power, as shown in Fig. S5 in the Supplementary Material. In comparison, these thermal-induced morphology changes cannot be observed in the gold plate even when the repetition rate is above 20 kHz due to its high thermal conductivity and melting point.

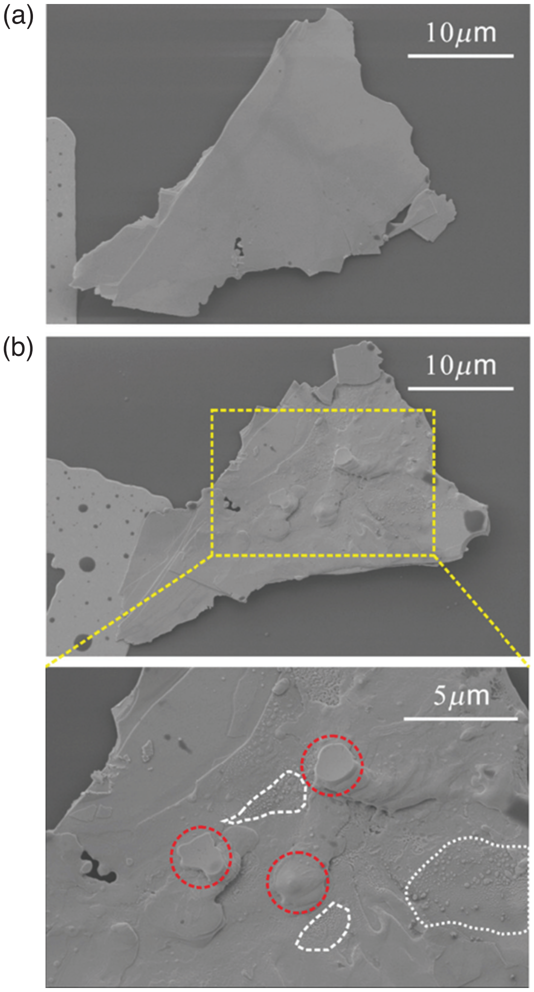

Fig. 5 SEM images of a Sb_2Te_3 plate (a) before and (b) after motion. The red and white dashed circles in (b) mark formed microbumps and a myriad of small spheres, respectively.

To better visualize the formed microbumps, we compare two SEM images of a Sb_2Te_3 plate before and after the unstable motion. Figure 5(a) shows that the surface of the plate before the motion is rather flat. Contrastingly, Fig. 5(b) shows that, after the motion, several microbumps (marked with red dashed circles) are induced as expected due to the Marangoni effects. Moreover, a myriad of small spheres is observed in the colder peripheral regions (marked with white dashed circles) potentially due to the dewetting effects.[33] Further, to observe the microbumps formed in larger areas, we transferred a Sb_2Te_3 plate onto a fiber endface (SMF-28, from Corning Company). The fiber core and the plate overlap each other. The nanosecond laser pulses are guided through the fiber and impinge on the plate directly. Similar observations as in Fig. 5 are given in Fig. S6 in the Supplementary Material.

5 Liquid-Like Motion

In addition to the induced motion instability shown in Fig. 4, the thermal effects lead to a new type of liquid-like motion. This liquid-like motion exhibits several features completely different from the spiral motion that is known to be driven by elastic waves, thus being worthy of discussion.

First, the onset of this liquid-like motion must require a high-pulse repetition rate [e.g., 11.5 kHz in Fig. 6]. Consequently, the shape of the Sb_2Te_3 plate is strongly deformed [see Fig. 6(a)]. The Marangoni effects induce a large microbump that contacts the microfiber [marked with a black rectangle in Fig. 6(a)], and the microbump is heated to viscoelasticity (molten-like) states. During the motion, the microbump deforms its shape periodically, accompanying the asymmetry in the left and right contact angles [see Fig. 6(b)]. This characteristic feature well resembles the motion of a liquid droplet: the unbalanced Young's force, manifesting in asymmetric contact angles, drives the motion (see Note S2 in the Supplementary Material for detailed analysis).[34] For this reason, the observed motion is termed liquid-like motion.

Second, the motion speed is significantly slower than the spiral motion. Figure 6(c) shows that the motion speed is only about 120 nm/s. Recalling that the pulse repetition rate is 11.5 kHz, the motion distance per pulse is about 0.01 nm, which is even below the atomic scale. This implies that the physics occurring in a single pulse is somehow insignificant to the observed macroscopic motion. Instead, the essential motion dynamics, which feature classical mechanics at the macroscopic scale (that is, the motion distance at least exceeds atomic lattice sizes), should occur in a longer time scale involving multiple pulses. In view of this, we deduce that this liquid-like motion is a multiple-pulse phenomenon instead of a single-pulse phenomenon as is for the elastic-waves-driven spiral motion.

Third, in all the observations of such liquid-like motions, we find that, besides the large microbump that contacts the microfiber, there also exist suspended, small ones close to the microfiber [marked with circles in Figs. 6(a) and 6(e)]. As is shown in Fig. 6(d), the suspended microbump vibrates in the vertical direction periodically by the surface adhesion of the microfiber.

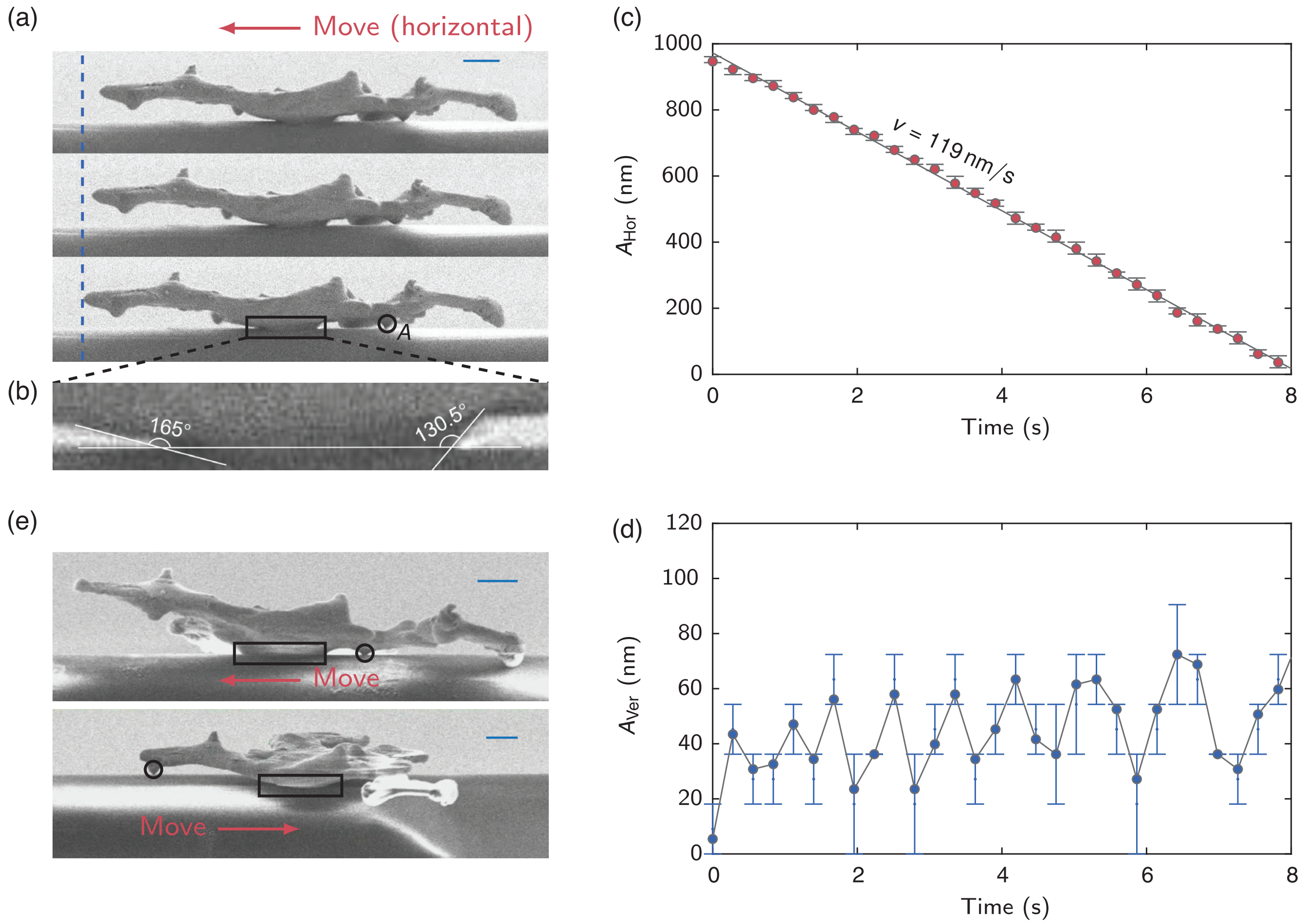

Fig. 6 Liquid-like motion of Sb_2Te_3 plates on microfibers. (a) Time sequencing SEM images of a Sb_2Te_3 plate showing liquid-like motion. The used supercontinuum laser pulse has 5.4-mW average power and 11.5-kHz repetition rate. A large microbump contacting with the microfiber and a small one is marked with a rectangle and circle, respectively (Video 4, MP4, 895 kB [URL: https://doi.org/10.1117/1.APN.1.2.026005.s4]). (b) Zoomed-in microbump [corresponding to the marked rectangle in (a)] showing asymmetric contact angles. Scale bar: 1 μm. (c) Horizontal and (d) vertical displacements of the point A in the Sb_2Te_3 plate as functions of time. The point A is labeled in (a). (e) Two exemplified samples show that horizontal motion direction of the plates points from a small microbump close to the microfiber (marked with circle) to a large one contacting with the microfiber (marked with rectangle). Scale bars: 1 μm (Video 5, MP4, 7.90 MB [URL: https://doi.org/10.1117/1.APN.1.2.026005.s5]).

Simultaneously, the structure moves horizontally. The horizontal translation thus hybrids with the vertical vibration.

Finally, the horizontal motion of the plate is universally observed to be along the direction pointing from the suspended microbump to the contacted one, as is illustrated with three different samples in Figs. 6(a) (Video 4) and 6(e) (Video 5). However, a satisfactory, quantitative interpretation is not trivial due to the involvements of complicated material states of high temperature, interfacial interactions, and temperature- and surfactant-modified surface tensions. Nevertheless, a phenomenological explanation without referring to its underlying microscopic mechanisms may be because the vertical vibration of the suspended microbump leads to the periodic deformation of the contacted microbump (see Videos 4 and 5), which generates the unbalanced Young's force in the same direction as the horizontal motion [see Note S2 in the Supplementary Material].

6 Conclusions

In summary, light-induced locomotion of microsized topological insulator Sb_2Te_3 plates along silica microfibers is demonstrated. The motion speed is controlled by tuning the average power of incident laser pulses. Our results confirm the validity of the previously established actuation principle based on light-induced elastic waves, and supplement previous demonstrations with gold microplates. We expect that this straightforward validation may encourage researchers to exploit this concept for more challenging application-oriented tasks, e.g., in integrated photonic circuits, wherein mobile microobjects can be precisely transported to targeted positions in circuits for user-defined functionalities, such as optical switches/modulators. Moreover, the thermal effects on actuation are examined. We observe the formations of the microbumps on the surfaces of the plates due to the Marangoni effects, and reveal their induced motion instability and a new type of liquid-like motion.

Acknowledgments

This work was supported by the National Natural Science Foundation of China (Nos. 61927820, 61905201, and 62275221). The authors thank Westlake Center for Micro-Nano Fabrication for the facility support and technical assistance.

References

1. S. Palagi et al., "Structured light enables biomimetic swimming and versatile locomotion of photoresponsive soft microrobots," *Nat. Mater.* **15**, 647 (2016).
2. X. Ma et al., "Enzyme-powered hollow mesoporous Janus nanomotors," *Nano Lett.* **15**, 7043 (2015).
3. D. Fan et al., "Subcellular-resolution delivery of a cytokine through precisely manipulated nanowires," *Nat. Nanotechnol.* **5**, 545 (2010).
4. M. M. Wang et al., "Microfluidic sorting of mammalian cells by optical force switching," *Nat. Biotechnol.* **23**, 83 (2005).
5. M. Z. Miskin et al., "Electronically integrated, mass-manufactured, microscopic robots," *Nature* **584**, 557 (2020).
6. D. G. Grier, "A revolution in optical manipulation," *Nature* **424**, 810 (2003).
7. M. P. MacDonald, G. C. Spalding, and K. Dholakia, "Microfluidic sorting in an optical lattice," *Nature* **426**, 421 (2003).
8. J. Ahn et al., "Optically levitated nanodumbbell torsion balance and GHz nanomechanical rotor," *Phys. Rev. Lett.* **121**, 33603 (2018).
9. T. M. Hoang et al., "Electron spin control of optically levitated nanodiamonds in vacuum," *Nat. Commun.* **7**, 12250 (2016).
10. J. Millen et al., "Optomechanics with levitated particles," *Rep. Prog. Phys.* **83**, 026401 (2020).
11. J. Gieseler et al., "Dynamic relaxation of a levitated nanoparticle from a non-equilibrium steady state," *Nat. Nanotechnol.* **9**, 358 (2014).
12. A. Ashkin, "Acceleration and trapping of particles by radiation pressure," *Phys. Rev. Lett.* **24**, 156 (1970).
13. S. L. Neale et al., "All-optical control of microfluidic components using form birefringence," *Nat. Mater.* **4**, 530 (2005).
14. D. Gao et al., "Optical manipulation from the microscale to the nanoscale: fundamentals, advances and prospects," *Light: Sci. Appl.* **6**, e17039 (2017).
15. K. Kendall, "Adhesion: molecules and mechanics," *Science* **263**, 1720 (1994).
16. J. Lu et al., "Light-induced pulling and pushing by the synergic effect of optical force and photophoretic force," *Phys. Rev. Lett.* **118**, 043601 (2017).
17. J. Lu et al., "Nanoscale lamb wave-driven motors in nonliquid environments," *Sci. Adv.* **5**, eaau8271 (2019).
18. S. Linghu et al., "Plasmon-driven nanowire actuators for on-chip manipulation," *Nat. Commun.* **12**, 385 (2021).
19. W. Tang et al., "Micro-scale opto-thermo-mechanical actuation in the dry adhesive regime," *Light: Sci. Appl.* **10**, 193 (2021).
20. W. Lyu et al., "Light-induced in-plane rotation of microobjects on microfibers," *Laser Photonics Rev.* **16**, 2100561 (2022).
21. M. K. Kurosawa, M. Takahashi, and T. Higuchi, Elastic contact conditions to optimize friction drive of surface acoustic wave motor, *IEEE Trans. Ultrason. Ferroelectr. Freq. Control* **45**, 1229 (1998).
22. T. Shigematsu, M. K. Kurosawa, and K. Asai, "Nano meter stepping drive of surface acoustic wave motor," in Proc. IEEE Conf. Nanotechnol., Vol. 50, p. 495 (2001).
23. H. Zhang et al., "Topological insulators in $\mathrm{Bi_2Se_3}$, $\mathrm{Bi_2Te_3}$, and $\mathrm{Sb_2Te_3}$ with a single dirac cone on the surface," *Nat. Phys.* **5**, 438 (2009).
24. Z. Jiang et al., "Enhanced spin Seebeck effect signal due to spin-momentum locked topological surface states," *Nat. Commun.* **7**, 11458 (2016).
25. Y. Xu, Z. Gan, and S. C. Zhang, "Enhanced thermoelectric performance and anomalous seebeck effects in topological insulators," *Phys. Rev. Lett.* **112**, 226801 (2014).
26. J. Y. Ou et al., "Ultraviolet and visible range plasmonics in the topological insulator $\mathrm{Bi_{1.5}Sb_{0.5}Te_{1.8}Se_{1.2}}$," *Nat. Commun.* **5**, 5139 (2014).
27. V. A. Kul'bachinskii et al., "A tunneling spectroscopy study of the temperature dependence of the forbidden band in $\mathrm{Bi_2Te_3}$ and $\mathrm{Sb_2Te_3}$," *J. Exp. Theor. Phys.* **97**, 1212 (2003).
28. R. Wang, J. Wei, and Y. Fan, "Chalcogenide phase-change thin films used as grayscale photolithography materials," *Opt. Express* **22**, 4973 (2014).
29. H. Lu et al., "Magnetic plasmon resonances in nanostructured topological insulators for strongly enhanced light–$\mathrm{MoS_2}$ interactions," *Light: Sci. Appl.* **9**, 191 (2020).
30. W. Richter and C. Becker, "A Raman and far-infrared investigation of phonons in the rhombohedral V2–VI3 compounds $\mathrm{Bi_2Te_3}$, $\mathrm{Bi_2Se_3}$, and $\mathrm{Sb_2Te_3}$ and $\mathrm{Bi_2(Te_{1-x}\,Se_x)_3}$ $(0 < x < 1)$, $\mathrm{(Bi_{1-y}Sb_y)_2Te_3}$ $(0 < y < 1)$," *Physica Status Solidi (b)* **84**, 619 (1977).
31. Z. Yue et al., "Nanometric holograms based on a topological insulator material," *Nat. Commun.* **8**, 15354 (2017).
32. A. Dun, J. Wei, and F. Gan, "Marangoni effect induced micro/nano-patterning on $\mathrm{Sb_2Te_3}$ phase change thin film by laser pulse," *Appl. Phys. A: Mater. Sci. Process.* **103**, 139 (2011).
33. C. V. Thompson, "Solid-state dewetting of thin films," *Annu. Rev. Mater. Res.* **42**, 399 (2012).
34. F. Brochard, "Motions of droplets on solid surfaces induced by chemical or thermal gradients," *Langmuir* **5**, 432 (1989).
35. B. Torrie, "Raman spectrum of tellurium," *Solid State Commun.* **8**, 1899 (1970).
36. Q. Wu et al., "Two-dimensional semiconducting and single-crystalline antimony trioxide directly-grown on monolayer graphene," *Chem. Commun.* **55**, 2473 (2019).

Biographies of the authors are not available.